nature nanotechnology

REVIEW ARTICLE

PUBLISHED ONLINE: 5 AUGUST 2014 | DOI: 10.1038/NNANO.2014.157

Advanced scanning probe lithography

Ricardo Garcia[1], Armin W. Knoll[2] and Elisa Riedo[3]*

The nanoscale control afforded by scanning probe microscopes has prompted the development of a wide variety of scanning-probe-based patterning methods. Some of these methods have demonstrated a high degree of robustness and patterning capabilities that are unmatched by other lithographic techniques. However, the limited throughput of scanning probe lithography has prevented its exploitation in technological applications. Here, we review the fundamentals of scanning probe lithography and its use in materials science and nanotechnology. We focus on robust methods, such as those based on thermal effects, chemical reactions and voltage-induced processes, that demonstrate a potential for applications.

Progress in nanotechnology depends on the capability to fabricate, position and interconnect nanometre-scale structures. A variety of materials and systems such as nanoparticles, nanowires, plasmonic materials and organic semiconductors, as well as two-dimensional materials such as graphene and transition-metal dichalcogenides are finding applications in nanoelectronics, nanophotonics, organic electronics and biomedical applications. The success of many of the above applications relies on the existence of suitable nanolithography approaches. However, patterning materials with nanoscale features aimed at improving integration and device performance poses several challenges. The limitations of conventional lithography techniques related to resolution, operational costs and lack of flexibility to pattern organic and novel materials have motivated the development of unconventional fabrication methods[1–3].

Since the first patterning experiments performed with a scanning probe microscope in the late 1980s, scanning probe lithography (SPL) has emerged as an alternative type of lithography for academic research that combines nanoscale feature-size, relatively low technological requirements and the ability to handle soft matter, from small organic molecules to proteins and polymers. Scanning probe lithography experiments have provided striking examples of its capabilities such as the ability to pattern three-dimensional relief structures with nanoscale features[4], the fabrication of the smallest field-effect transistor[5] or the patterning of proteins with 10-nm feature size[6].

Figure 1a shows a general scheme of SPL operation. There is a variety of approaches to modify a material at the probe/surface interface, which have generated several SPL methods. Scanning probe lithographies can be either classified by emphasizing the distinction between the general nature of the process, chemical versus physical, or by considering if SPL implies the removal or addition of material. However, we consider it is more inclusive and systematic to classify the different SPL methods in terms of the driving mechanisms used in the patterning process, namely thermal, electrical, mechanical and diffusive (Fig. 1b).

Challenges in nanoscale lithography

The workhorse of large-volume complementary metal–oxide–semiconductor fabrication, optical lithography at a wavelength of 192 nm, has reached the physical limits in terms of minimal achievable pitch of a single patterning run of about 80 nm. To make denser integrated circuits and additionally to keep Moore's law fulfilled for feature sizes approaching the single-digit nanometre range, multi-patterning extensions such as double- and triple-patterning have been introduced with the acceptance of the inherently higher manufacturing costs. Alternatively, the technically challenging switch to shorter wavelengths in the extreme ultraviolet spectrum at 12.5 nm is considered a viable although extremely costly possibility for the next years[7].

Economic reasons dictate throughputs of more than 100 wafers per hour corresponding to $>10^{12}$ μm^2 h^{-1} for high-volume-production techniques (Fig. 2a). This mask-based high-volume lithography environment requires accompanying techniques for flexible low-volume production, mask fabrication and prototyping of the next-generation devices. These applications require versatile tools without the overhead to produce masks for each patterning step, so called maskless lithography technologies. Their throughput scales phenemenologically with the achievable resolution according to a power law as was first recognized by Tennant[8]. Among the maskless methods the dominating technique is electron-beam lithography (blue shapes in Fig. 2a), which uses a Gaussian electron beam or variable shaped beams for sub-20-nm resolution or high-throughput demands, respectively. At high resolutions, the trade-off between resolution and throughput is determined by the sustainable beam current and resist sensitivity. Both higher currents and enhanced sensitivity through chemical amplification (chemically amplified resists) lead to a reduction in resolution, limiting the throughput at high resolutions. Even higher resolutions in the single-digit nanometre range can be obtained by using inorganic resists or electron-beam-induced deposition[9], albeit at very limited throughputs of about 1 μm^2 h^{-1} and high costs. At present, massively parallel approaches are under study with the goal to scale electron-beam lithography towards high-volume production[10,11]. At the same time alternative nanopatterning methods have been explored. Novel beam-based methods using He (ref. 12) and Ne (ref. 13) ions instead of electrons promise high resolution and enhanced resist sensitivity.

In parallel to the developments of beam-based methods, SPL methods are receiving renewed interest because of their flexibility to handle novel materials, and their inherent inspection and positioning capabilities. Since their invention, scanning probe microscopes have been used to image, modify and manipulate surfaces at the nanometre and atomic scales. Atomic-scale manipulations have been performed in ultrahigh vacuum although the exceedingly small throughput values (Fig. 2a) greatly limit their impact

[1]Instituto de Ciencia de Materiales de Madrid, CSIC, Sor Juana Inés de la Cruz 3. 28049 Madrid, Spain, [2]IBM Research - Zurich, Saeumerstr. 4, 8803 Rueschlikon, Switzerland, [3]School of Physics, Georgia Institute of Technology, Atlanta, Georgia 30332-0400, USA.
*e-mail: riedo@gatech.edu

© 2014 Macmillan Publishers Limited. All rights reserved

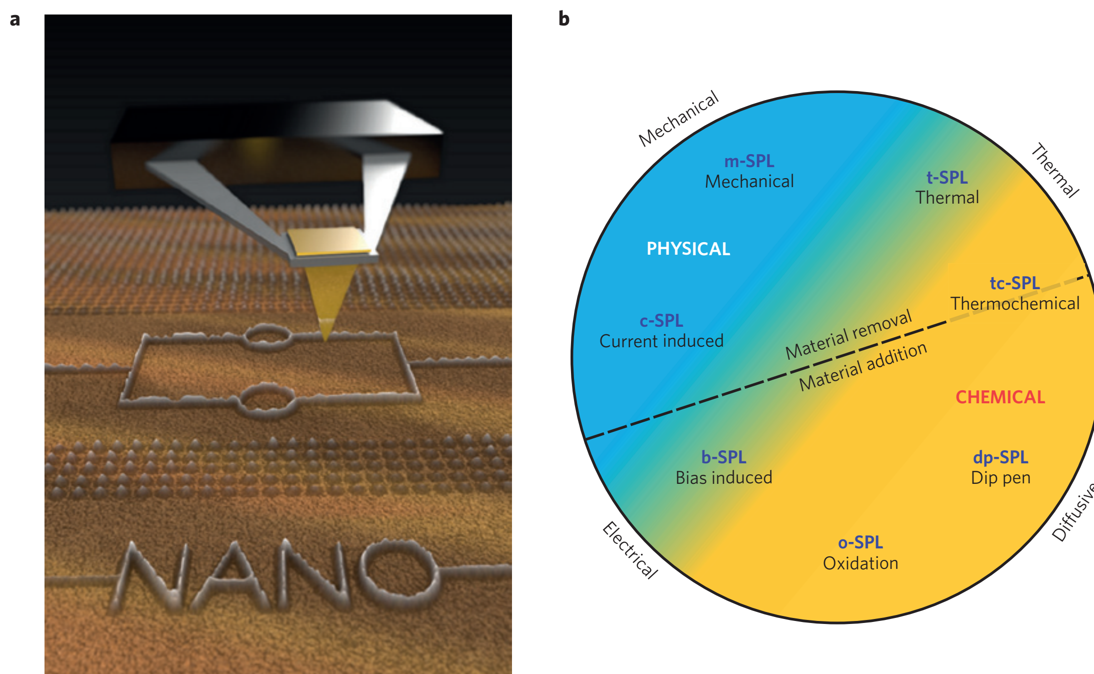

Figure 1 | Scanning probe lithography. a, Schematic of scanning probe lithography (SPL) where imaging and patterning applications are orthogonal. **b**, Classification of SPL methods according to the dominant tip–surface interaction used for patterning, namely electrical, thermal, mechanical and diffusive processes.

and applications. Recent developments with techniques operating in ambient atmosphere have shown that some scanning probe nanolithography approaches could also be competitive in terms of resolution, throughput and versatility of the materials that can be patterned. This makes SPL an appealing type of nanolithography for research and some niche technological applications. For example, thermal SPL has achieved a resolution of 10 nm while the throughput is in the 10^4–10^5 μm^2 h^{-1} range.

The role of scanning probe lithography

Scanning probe lithography includes several approaches to pattern materials with nanoscale resolution (Fig. 1b). These approaches have a common thread, which is the use of a sharp scanning probe to produce local modifications on a surface. The variety of SPL approaches arises from two main factors. First, the wealth of processes that could be controlled by using a sharp probe in contact or near contact with a nanoscale region of a sample surface. The processes involved include mechanical, thermal, electrostatic and chemical interactions, or different combinations of them. Second, the various methods that control the position of the scanning probe relative to the underneath surface, for example, through quantum tunnelling between the probe and a conductive surface as in the scanning tunnelling microscope, or by controlling the force between the probe and the surface as in the standard atomic force microscope (AFM). In fact, most of the current SPL methods rely on the use of an AFM.

The potential and variety of the methods available to scanning probe microscopy to locally modify surfaces was already evident in the early experiments. However, many of those approaches albeit inspirational because of their atomic-scale manipulation capabilities have been proven to be unpractical for any large-scale patterning or device applications. In this Review, the focus is on the SPL methods that are robust and versatile enough to make patterns and/or devices with a high degree of reproducibility and show a potential for scalability and compatibility with ambient conditions and novel materials. These methods are collectively called advanced SPL.

Compared with other techniques such as electron-beam lithography, the principal advantage of SPL is that it is a single-step process with sub-10-nm resolution. Most of the SPL writing processes are 'direct write' in nature, creating structures without the need for subsequent development steps. This is, in particular, relevant for a direct patterning or conversion of functional materials such as graphene or other two-dimensional materials, which are known for being sensitive to resist residues[14]. Most SPL methods operate under (controlled) atmospheric conditions, which reduces the tool overhead and cost, and facilitates applications. The constituents of the atmosphere may even provide the functionality for some SPL methods such as for bias SPL or oxidation SPL. The simplicity of the techniques also allows for straightforward parallelization schemes. Furthermore, the scanning probe microscope is capable of detecting surface features down to atomic resolution. In contrast to beam-based methods, imaging and patterning in SPL are orthogonal, that is, the imaging process neither influences the written structures nor involves a partial writing operation. Together, the non-destructive imaging capability and the direct writing enables the concept of so-called closed-loop lithography to be established, that is, a lithography tool with inherent feedback of the writing result to optimize the writing stimuli during the patterning process. This tool is thus capable of autonomously controlling the writing process, improving dramatically the ease of use to create complex and high-resolution nanoscale structures.

In general, the ability of SPL to image the surface of a material, to fabricate complex patterns *in situ* with sub-10-nm precision in size and single-nanometre accuracy in positioning, and to allow post-patterning *in situ* metrology is rather unique. Finally, SPL is capable of patterning a large variety of materials, including polymers and biological matter. Applications of SPL to pattern silicon[15], graphene[16], piezoelectric/ferroelectric ceramics[17], polymers[4,18–21] and proteins[6] have been demonstrated. The capability of using the same SPL set-up to pattern different materials at the same time is also very appealing[22].

Thermal and thermochemical SPL

Thermal SPL (t-SPL) was first developed for data-storage purposes in the early 1990s[23]. In that work it was understood that the

© 2014 Macmillan Publishers Limited. All rights reserved

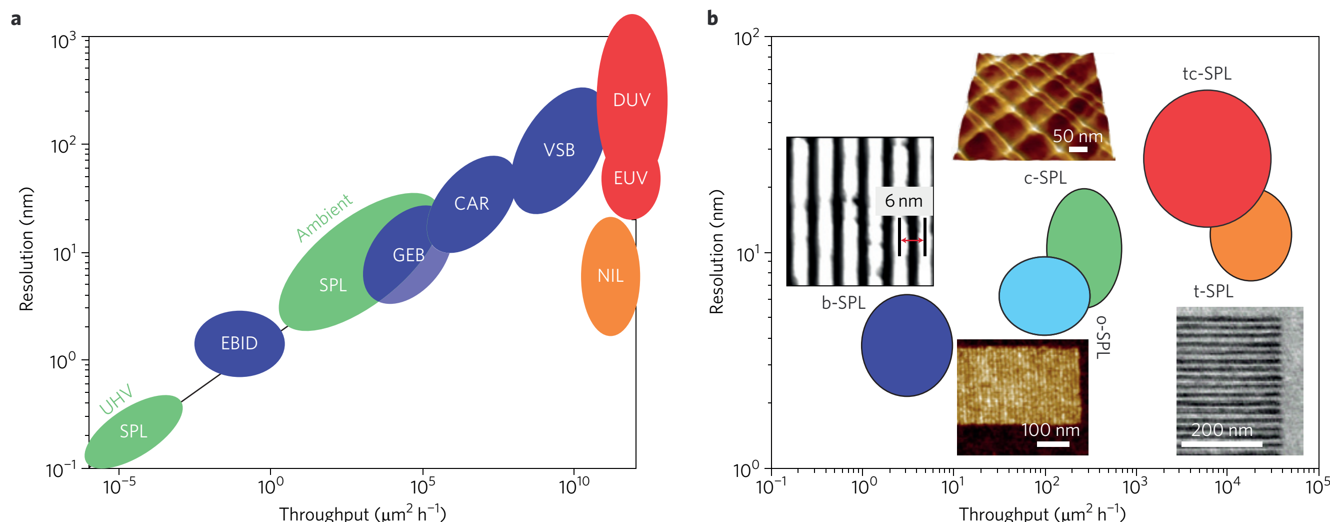

Figure 2 | Nanofabrication landscape. a, Resolution and throughput in nanolithography. High-volume techniques (red shapes) require throughput values >10^{12} μm² h⁻¹. At lower throughput, maskless electron beam (blue shapes) and scanning probe techniques (green shapes) converge roughly on a single line, called Tennant's law. GEB, Gaussian beam lithography; EBID, electron-beam-induced deposition; CAR, chemically amplified resists; VSB, variable shaped beam; DUV, deep ultraviolet; EUV, extreme ultraviolet; NIL, nanoimprint lithography; UHV, ultrahigh vacuum. **b**, Within the advanced scanning probe techniques (ambient SPL in **a**) a similar correlation exists. High-resolution results are shown for bias-induced scanning probe lithography (b-SPL), oxidation SPL (o-SPL), current-controlled SPL (c-SPL) and thermal SPL (t-SPL). tc-SPL, thermochemical SPL. Figure reprinted with permission from: **a**, ref. 8, © Springer; **b**, images for b-SPL, ref. 61, © American Chemical Society; c-SPL, ref. 51, © SPIE; t-SPL, ref. 27, © American Chemical Society.

transport of heat is only significant if the tip and the sample are in intimate contact. Thus, the heat is highly localized at the tip–sample contact area, which is of the order of a few nm² due to the nanoscale dimensions of the apex of the scanning probe microscope tip. Furthermore, similar to the case of light, manipulation by heat does not require the presence of conductive surfaces and thus is widely applicable.

Heat is used in t-SPL to modify a material mechanically. In thermochemical SPL (tc-SPL), also known as thermochemical nanolithography, heat is used to locally change the chemistry of a material[24,25]. In the early experiments, laser heating with pulse times of microseconds and linear scan speeds of 25 mm s⁻¹ demonstrated the high-speed potential of thermomechanical writing schemes. Today, heaters integrated into silicon cantilevers are used (Fig. 3a), which facilitates the control of the writing parameters and improves the resolution. The tip is resistively heated by a current flowing in the cantilever legs, which are highly doped except for the region where the tip is positioned. In silicon, the maximum sustainable temperature at the heater position is limited by electromigration of the dopants to 800–1,000 °C, depending on the type of dopant. Typical thermal time constants of the integrated heaters range from 5 to >100 μs (ref. 24), allowing for fast switching of the thermal stimulus. The effective temperature at the substrate surface depends on the ratio of thermal resistance of the substrate and of the combined resistance of the tip and tip/sample interface[24]. For sharp tips with radii on the order of 5 nm, and polymer films thicker than the lateral size of the contact, the temperature of the heater is reduced by about a factor of two at the polymer surface. Thus, highly temperature sensitive materials are required for high resolution. We also note that, in ambient conditions, the thermal heater may also act as a height sensor and imaging can be achieved by using only electrical control without the need for an optical-lever set-up.

Figure 3 summarizes some recent achievements in t-SPL. In all cases presented the highly localized heat stimulus is used to trigger a nanoscale reaction, which consists of excitation or cleavage of physical or chemical bonds, as well as more complex reactions such as crystallization processes. We distinguish the thermal patterning methods according to the characteristics of the created patterns. If the thermal process results in efficient removal of material for the purpose of generating a topographical pattern, the method is termed t-SPL. If the process is purely thermochemical in nature[25] and the resulting patterns are made of a material with structure and chemistry different from the original one, we term the method tc-SPL. In t-SPL[26,27] either molecular glass resists[4] or the thermally responsive polymer poly(phthalaldehyde)[28] are used as a substrate, and they perform exceptionally well for topographic patterning. In poly(phthalaldehyde), the fission of a single bond is amplified by spontaneous decomposition of the remaining polymer chains resulting in a highly efficient patterning process. The patterns shown in Fig. 3b contain 880 × 880 pixels and were written in less than 12 seconds, demonstrating the high throughput of the approach[29]. Throughputs are in the range of 5×10^4 μm² h⁻¹ (Fig. 2b). Patterning at a half pitch down to 10 nm without proximity corrections was demonstrated[27]. Other milestones towards technical readiness of the technique are the stitching of patterning fields at <10 nm precision[30] and a high-quality pattern transfer into the underlying silicon substrate at high resolution and low line edge roughness (Fig. 3c)[27].

A key example of tc-SPL is the use of hot probes for on-demand patterning of field-effect transistors from a pentacene precursor as shown in Fig. 3d[31]. Thermal reduction of functionalized graphene by tc-SPL is also perceived as an attractive way to pattern graphene with nanoscale precision. Reduced graphene oxide[32] (Fig. 3e) and reduced graphene fluoride[33] nanoribbons have been fabricated with a width as low as 12 nm and tunable conductivity over four orders of magnitude. Field-effect transistors have also been demonstrated by using these nanowires. Furthermore, direct writing of ferroelectric and/or piezoelectric ceramic nanostructures on plastic, glass and silicon was demonstrated by local tc-SPL-induced crystallization[17] (Fig. 3f). Recently, tc-SPL was also used to deprotect active groups such as carboxylic acid[25,34] and amine groups[35], which can subsequently be used for biochemical conjugation of nano-objects. Multifunctional patterns of proteins, DNA and C_{60} have been obtained with a resolution down to 10 nm at patterning speeds up to millimetres per second[35].

© 2014 Macmillan Publishers Limited. All rights reserved

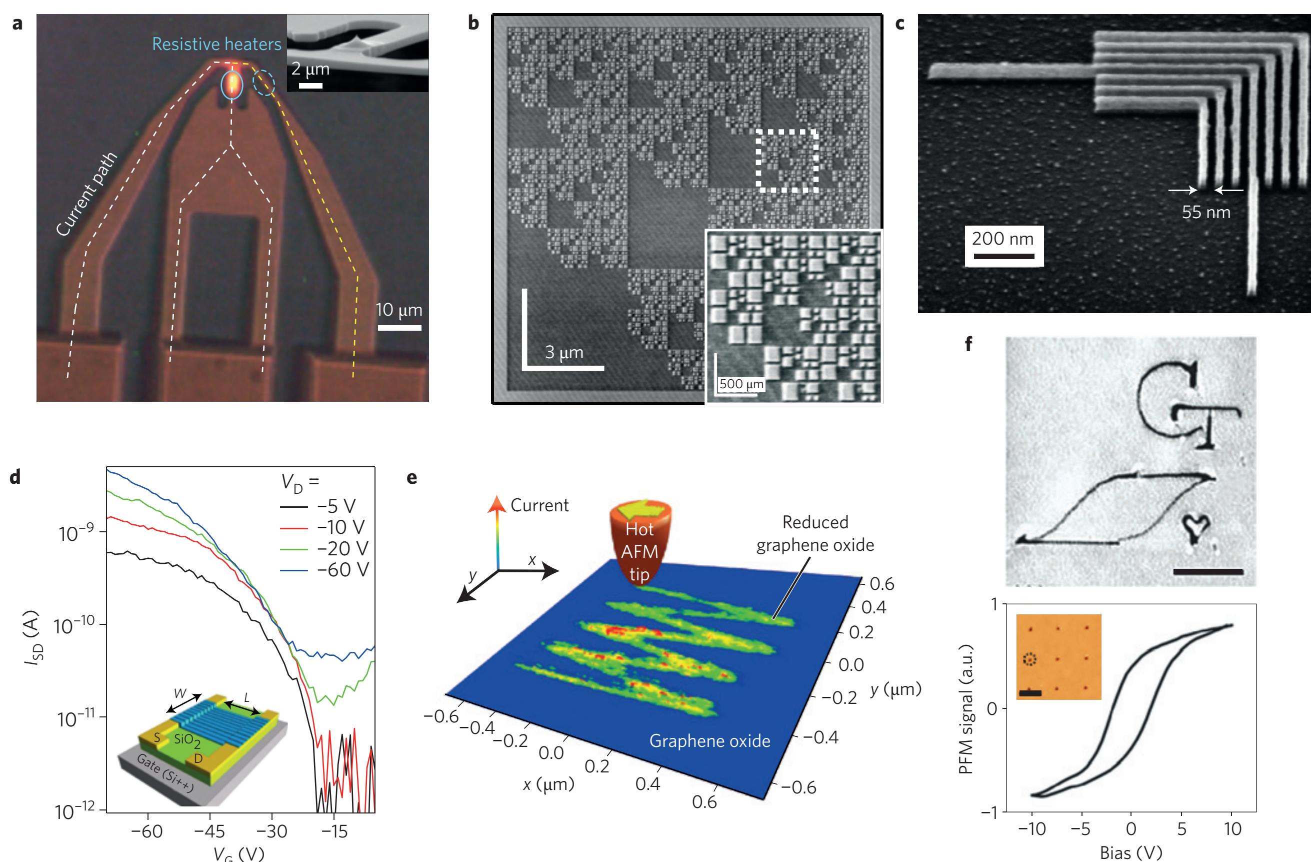

Figure 3 | Thermal and thermochemical scanning probe lithography. a, Silicon thermal cantilever comprising integrated joule heaters for tip heating and for thermal sensing. Inset: Scanning electron micrograph of the tip region of the cantilever. **b**, High-speed thermal scanning probe lithography (t-SPL). Topographical image of a fractal pattern comprising 880 × 880 pixels written in 12.8 seconds[29]. **c**, Silicon structures created from a reactive ion etching transfer of t-SPL-written nested L-lines at 27-nm half-pitch[27]. **d**, Direct patterning of field-effect transistors by conversion of a precursor material into pentacene[31]. Drain current, I_{SD}, plotted against gate voltage, V_g, for different drain voltage levels, V_D. Inset: Device configuration schematic. *W* and *L* are the width and length of the channel, respectively; S and D are the source and drain electrodes, respectively. **e**, Direct thermal conversion of graphene oxide to conductive graphene using thermochemical SPL (tc-SPL)[32]. **f**, Top: Local crystallization by tc-SPL of a precursor film on plastic or Si to form nanostructures of $PbTiO_3$ (PTO) ceramics. Scale bar, 1 µm. Bottom: Piezo-force-microscopy measurement of the typical ferroelectric hysteresis loop acquired on a PTO nanodot fabricated by tc-SPL, and shown in the inset[17]. Scale bar, 1 µm. Figure reprinted with permission from: **a**, ref. 126, © SPIE; **b**, ref. 29, © Institute of Physics; **c**, ref. 27, © American Chemical Society; **d**, ref. 31, © Wiley; **e**, ref. 32, © American Association for the Advancement of Science; **f**, ref. 17, © Wiley.

Greyscale chemical and topographical patterning. A particular strength of t-SPL and tc-SPL is the precise control of the patterning parameters at the nanometre-size scale and microsecond timescale. The control is due to the highly reproducible motion of the cantilever and thus the repeatability of the interaction times and forces, as well as the stability of the heater temperature. In the lithography application this high level of control enables the production of three-dimensional greyscale relief patterns[28] even on rough surfaces, as well as the production of chemical gradients[20] in a single patterning run. By exploiting the 'closed-loop lithography' scheme mentioned above, the absolute patterning depth in a poly(phthalaldehyde) film can be controlled to about single-nanometre precision, less than the linear dimension of a single resist molecule. An example is shown in Fig. 4a depicting the final topographical pattern imaged during the closed-loop writing process. Using the same colour scale, the inset shows the programmed bitmap, a portrait of Richard Feynman who in 1959 wrote a visionary essay about the possibilities of manipulating matter at the micro, nano and atomic scales. The precision achieved can be seen from the cross-sectional profiles of both bitmaps in the bottom panel of Fig. 4a. The three-dimensional shape of the topographical relief structures was exploited for a precise and oriented positioning of Au nanorods into t-SPL-defined guiding structures[36]. Figure 4b shows a scanning electron micrograph of bare Au nanorods placed with an accuracy of 10 nm on the silicon substrate after removal of the polymer template containing the guiding structures. Another application of the precise depth control is multilevel data storage, encoding three-bit levels into the depth of the indents[37]. A bit error rate of 10^{-3} could be achieved.

A similar control was obtained for the degree of chemical functionalization in a thermally sensitive polymer (Fig. 4c)[20]. The heated tip deprotects a functional group in the polymer to unmask primary amines, which serve as attachment sites for subsequent selective functionalization with the desired species of molecules and nano-objects. The density of amine groups on the surface is precisely controlled by the applied temperature and scanning speed, and can be predicted by using an Arrhenius model for the thermally activated chemical reaction. To visualize the programmed gradient of amines on the polymer surface, the deprotected functional amine groups are fluorescently labelled using a *N*-hydroxysuccinimide fluorescent dye and imaged with fluorescence microscopy. In Fig. 4c, we show the resulting optical image of a fluorescent 'Mona Lisa'. Other examples are the conversion of precursors into semiconducting polymers, thus enabling the direct three-dimensional writing of polymers relevant for organic electronics devices (Fig. 4d,e). This was first demonstrated by direct patterning of fluorescent structures from a poly-*p*-phenylene vinylene precursor material[18,19,22].

© 2014 Macmillan Publishers Limited. All rights reserved

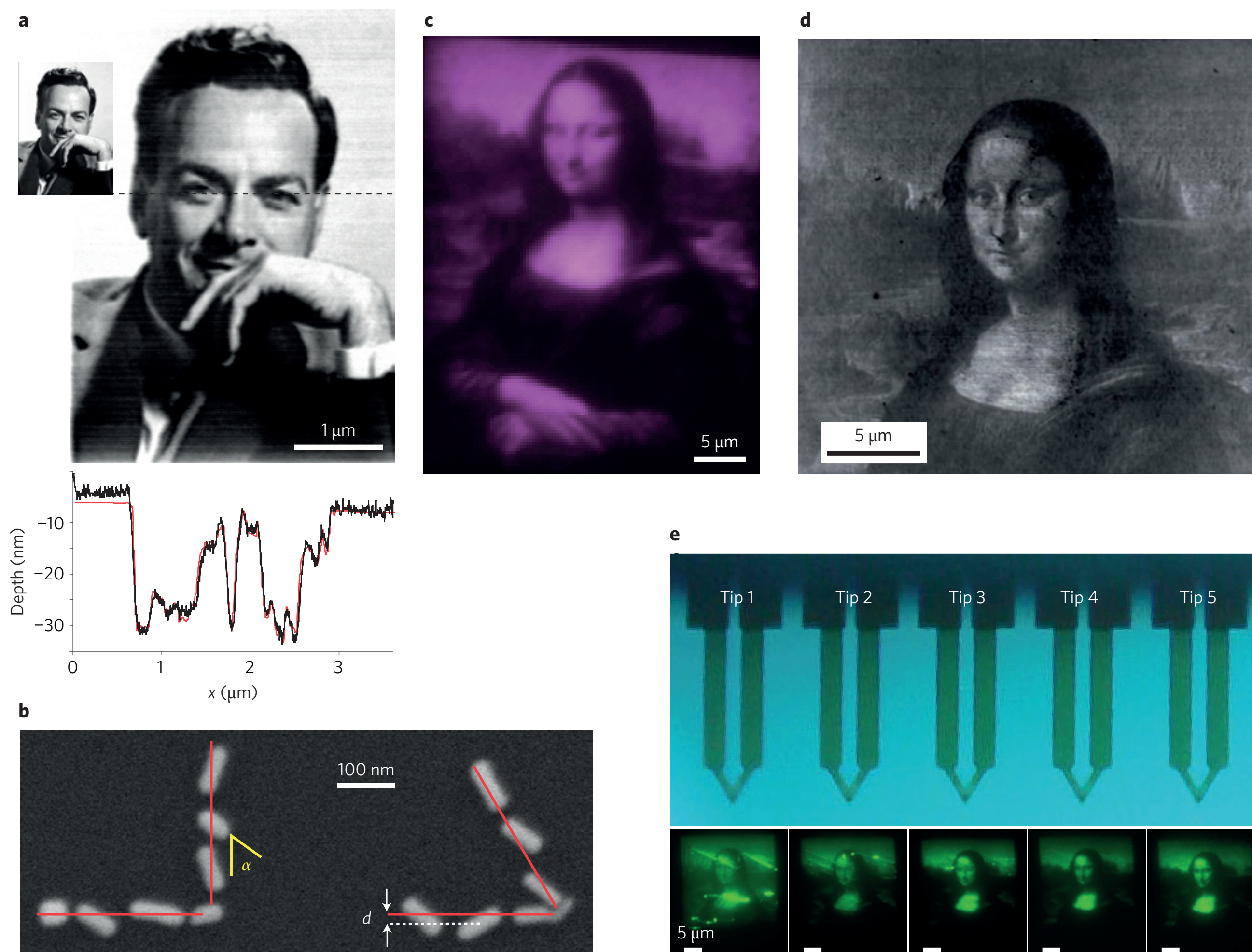

Figure 4 | Greyscale thermal and thermochemical scanning probe lithography. a, Greyscale patterning of a photograph of Richard Feynman (courtesy of the Archives, California Institute of Technology; used with the permission of Melanie Jackson Agency, LLC) with single-nanometre absolute depth precision written by closed-loop thermal scanning probe lithography (t-SPL). Inset: Programmed bitmap. Bottom: Cross-sectional profile of experimental data (black) and target pattern (red) taken along the dotted line. **b**, Precise positioning of Au nanorods on a silicon wafer after template removal[36]. The red lines mark the position of the guiding structures. A placement accuracy of 10 nm was achieved (standard deviation of the distance *d* from the centre of the guiding structures). The angle *α* indicates the largest error in rod alignment. **c**, Thermochemical SPL (tc-SPL) is used to control the density of amine groups on a polymer film. The thermally deprotected amines are then labelled with a fluorescent dye for visualization, showing in pink the optical fluorescence image of a Mona Lisa picture[20]. **d**, AFM topography image (full *z*-range 20 nm) of a three-dimensional Mona Lisa image nanopatterned by tc-SPL conversion of a precursor film into poly-*p*-phenylene vinylene (PPV)[22]. **e**, Image of an array of five thermal cantilevers and corresponding five fluorescence images of PPV Mona Lisa patterns obtained with the array[22]. Figure reprinted with permission from: **b**, ref. 36, © American Chemical Society; **c**, ref. 20, American Chemical Society; **d**,**e**, ref. 22, © Royal Society of Chemistry.

Bias-induced SPL

Force microscopy offers a flexible and versatile interface to control chemical processes at the nanoscale. The small size of the AFM tip's apex and the proximity of the surface facilitates the generation of extremely high electrical fields and, in conducting samples, a focused electron current. Remarkably, high electric fields ~10 V nm^{-1} (10 GV m^{-1}) can be achieved by applying moderate voltages (~10 V). Those fields and/or the associated electron currents are used to confine a variety of chemical reactions and/or to decompose gas[38,39] or liquid[40] molecules that lead to either a locally controlled deposition or to the growth of material on a surface. Furthermore, bias-induced SPL (b-SPL) experiments can be performed in ambient or liquid environments, which, in turn, increases the number of available chemical species.

There is a large variety of methods that combine the application of a voltage with a tip/surface interface to produce nanoscale features. The electric bias across the tip/surface interface can induce local and bulk electrochemical processes such as the anodic oxidation of semiconductors[41,42] and metals[42], as well as the reduction of earth metal oxides[43], metal salts[44] and ionic conductors[45]. Experimental schemes that are closer to the conventional electrochemical set-ups with reference, counter and working electrodes are also being used to deposit metal nanostructures[46,47]. In this context, b-SPL has been used to locally catalyse the reduction of insulating graphene oxide in the presence of hydrogen. Nanoribbons with widths ranging from 20 to 80 nm and conductivities of >10^4 S m^{-1} have been successfully generated, and a field-effect transistor was produced[48]. The method involves mild operating conditions, atmospheric pressure and low temperatures (≤115 °C). Oxidation SPL, the most robust and established nanolithography method of this kind, is described in the next section.

Bias-induced SPL can involve other processes such as field-induced deposition of matter[39,49–50], current-induced transformations[51,52] and desorption processes[42,53], as well as the direct

© 2014 Macmillan Publishers Limited. All rights reserved

deposition of charges[54] or the inversion of the polarization of a local volume in a ferroelectric film[55,56]. The atomic-scale resolution potential of b-SPL is illustrated by experiments reporting the local electron-induced hydrogen desorption on a Si(100) surface[53]. Using this method, clean and H-passivated regions on the surface have been produced. The chemical contrast between those regions has been combined to fabricate the smallest lithographically engineered electron devices[5,57,58].

The electric field at the tip/surface interface can invert the polarization of a small region in a ferroelectric film. This generates a non-volatile ferroelectric domain. This mechanism has been proposed for data storage[55,59,60]. The non-destructive write–erase process has achieved areal densities of 3.6 Tbit inch^{-2}.

Bias-induced SPL has also produced some other milestones such as the fabrication of the smallest pattern made at ambient pressure and room temperature on a silicon surface[61]. It has also been applied to integrate dissimilar materials with nanoscale accuracy such as germanium patterns on silicon surfaces[62]. The potential of b-SPL goes beyond the field of nanolithography. The method has been applied to understand new processes to decompose stable chemical species such as carbon dioxide[39]. These results expand and strengthen the applications of SPL and nanochemistry[45].

Oxidation SPL

The discovery of probe-based oxidation[41] was shadowed by the more exciting experiments reporting either modifications[62] or manipulations[63] of surfaces with atomic-scale capabilities[64,65]. However, the generality and robustness of the underlying chemical process (anodic oxidation) has transformed Dagata's observation into a reliable and versatile nanolithography approach for patterning and device fabrication[42]. Nanopatterning examples range from the generation of arrays of submicrometre lines and dots on crystalline surfaces[66–68], self-assembled monolayers[69–71] and polymers[72] to the fabrication of nanoscale templates for the growth of single-molecule magnets[73], proteins[6] and nanoparticles[74–76] to the directed self-assembly of block copolymers[77], polymer brush nanostructures[78], carbon nanotubes[79] or semiconductor nanostructures[80]. Examples of nanoscale devices and prototypes include, among others, single-photon detectors[81], photonic nanocavities[82], quantum devices (such as quantum point contacts[83,84], dots[85,86] and rings[87]) and several graphene devices[88–92]. A variety of transistors such as single-electron[93], metal-oxide[94] or nanowire field-effect transistors[15,95] have been fabricated by oxidation SPL (o-SPL). Other applications include the use of the local oxide as a coating to embed nanoparticles on a silicon surface[96]. Oxidation SPL is also contributing to bring a renewed interest to the physics of the water meniscus[97,98]. Oxidation SPL has received various names such as local oxidation nanolithography, scanning probe oxidation, nano-oxidation or local anodic oxidation.

The widespread academic use of o-SPL is explained by three features. First, the ability to nanopattern a wide variety of materials ranging from metals to semiconductors to self-assembled monolayers, and more recently to graphene or polymer-based resists. Second, its minimal technological requirements, which in combination with operation at room temperature and atmospheric pressure conditions, makes oxidation SPL very attractive for academic research. Third, the method is capable of performing many tasks concurrently, for example, at the same time it can generate a thin dielectric, a mask for further etching or a template to direct the growth of molecular architectures.

Oxidation SPL is based on the spatial confinement of an anodic oxidation reaction between the tip and the sample surface (Fig. 5a). The oxidation process is mediated by the formation of a nanoscale water bridge[99]. In fact, due to the sequential character of o-SPL the generation of a nanopattern might involve the formation of multiple water bridges. The role of the water meniscus is twofold. It acts as a nanoscale electrochemical cell that provides the oxyanions by which the reaction takes place (Fig. 5b). Second, it confines the reaction laterally, that is, the size of the meniscus determines the resolution of the features obtained by this technique[99]. The polarity of the voltage is in such a way that the tip acts as the cathode (negative) and the sample surface is the anode (positive). Oxidation SPL can be either performed with the tip in contact with the sample surface or in a non-contact mode.

The electric field has three roles in tip-based oxidation[42]. It induces the formation of the water bridge (Fig. 5c). Second, it generates the oxyanions needed for the oxidation by decomposing water molecules. Third, it drives the oxyanions to the sample interface and facilitates the oxidation process[100]. Ultrasmall silicon oxide nanostructures with a lateral size between 10 and 100 nm and a height in the 1 to 10 nm range have been generated using this technique. The main parameters that control the local oxidation process are the applied voltage (from a few volts to 20–30 V), the relative humidity (20%–80%), the duration of the process (10 μs–10 s), the tip–sample distance (2 nm–5 nm) and the scanning speed (0.5 μm s^{-1}–1 mm s^{-1}).

Molecular architectures. Selective oxidation and/or complete removal of self-assembled monolayers and subsequent surface functionalization of the oxidized regions have enabled the fabrication of nanoscale architectures[6,101]. Figure 5d,e illustrates the process to pattern linear arrays of proteins with a size that matches the molecular size of the protein, in this case ferritin. The process requires the functionalization of the silicon surface with an octadecyltrichlorosilane monolayer, then o-SPL is applied to pattern several silicon oxide lines on the surface. The process also removes the self-assembled monolayer in the regions exposed to the field. The patterned sample is immersed in a solution containing aminopropyltriethoxysilane (APTES) molecules until an APTES monolayer is deposited in the patterned lines. Then the sample is exposed to a solution containing ferritin molecules. At a pH above 5.3 the ferritin is negatively charged. Consequently, ferritin will be attracted towards the protonated amino-terminated regions of the APTES patterns. The ferritin molecules attached to the neutral octadecyltrichlorosilane areas are easily removed by rinsing the sample in buffer. The complete process gives rise to the formation of arrays of proteins with an accuracy that matches the size of the protein.

Nanoelectronic devices. To illustrate how o-SPL is applied to fabricate nanoelectronic devices we show some of the steps in the formation of silicon nanowire transistors and graphene quantum dots. The fabrication of a silicon nanowire transistor involves the patterning of a narrow oxide mask on top of the active layer of a silicon-on-insulator substrate[15,61,102] (Fig. 6a). The unmasked silicon layer is then removed by using wet or dry chemical etching procedures. The local oxide protects the underneath silicon from the etching. This leaves a single-crystalline silicon nanowire with a top width that matches the width of the oxide mask. Finally, the silicon nanowire is contacted to micrometre-sized platinum source and drain contacts by either photolithography or electron-beam lithography (Fig. 6b). The silicon nanowire can be transformed into a field-effect transistor by a third electrode that is usually at the back of the silicon substrate (Fig. 6c). This scheme has enabled the fabrication of label-free and ultrasensitive biosensors for the detection of the early stage of recombinational DNA repair by the RecA protein[103].

The fact that o-SPL does not require the use of resists that could modify the electronic properties of graphene has propitiated its application to fabricate a variety of graphene nanoscale devices. A graphene-based quantum dot has been fabricated[90] by locally oxidizing a graphene layer deposited on a silicon oxide surface (Fig. 6d). The microelectrodes are established by using shadow masking techniques. The quantum dot structure is generated by locally oxidizing regions in the graphene layer. Figure 6e shows the source and drain electrodes as well as the gates and the region occupied

© 2014 Macmillan Publishers Limited. All rights reserved

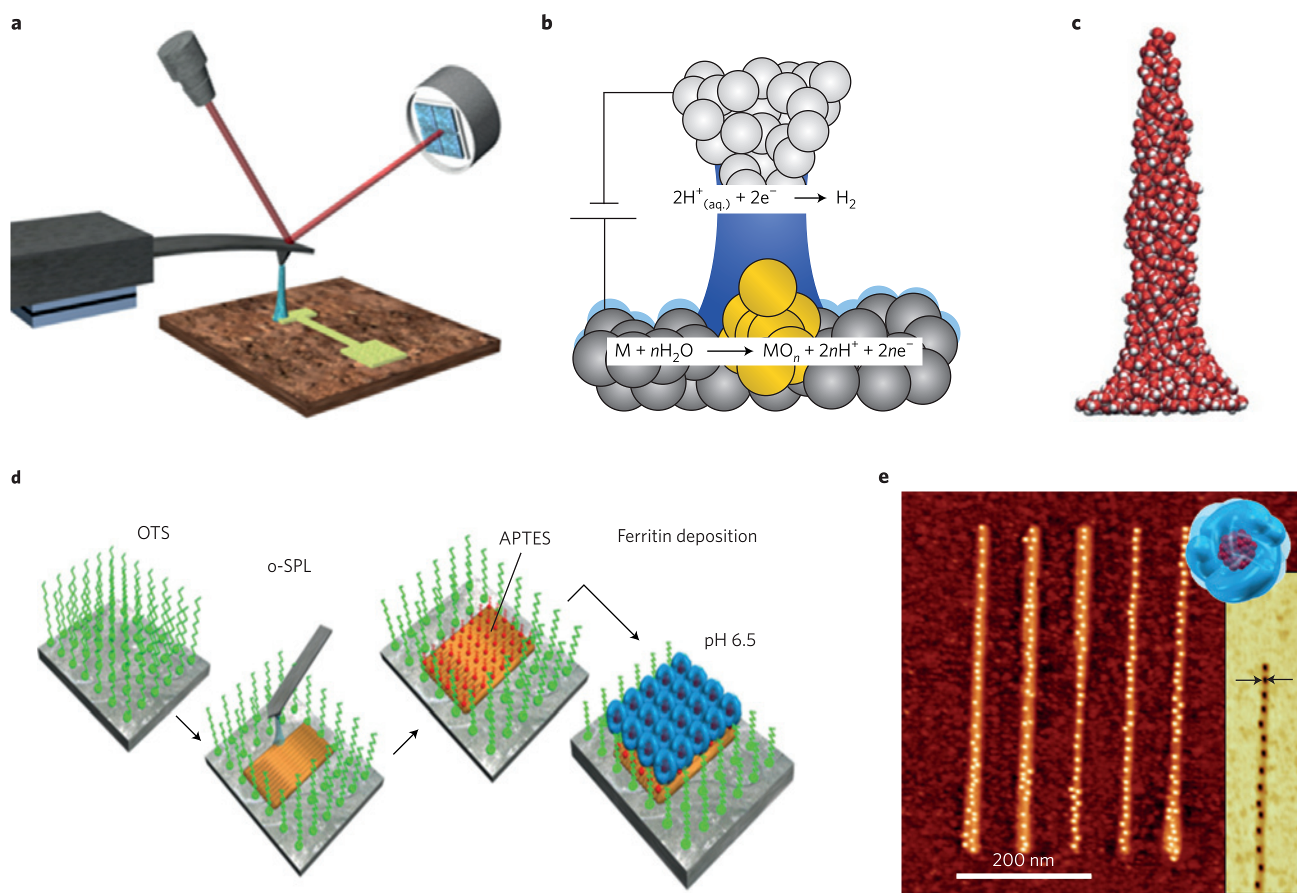

Figure 5 | Oxidation scanning probe lithography. a, The oxidation process used in oxidation SPL (o-SPL) is mediated by the formation of a water bridge that provides the oxyanions. The effective width of the liquid bridge together with the kinetics controls the feature size. **b**, General electrochemical reactions in local anodic oxidation. **c**, Molecular dynamics snapshot of the field-induced formation of a 2.5-nm-long water bridge (1,014 water molecules). Oxygen atoms are in red and hydrogen in white. **d**, Main steps to pattern ferritin proteins on a silicon surface by combining bottom-up electrostatic interactions and local oxidation. The silicon oxide pattern made on the silicon surface is shown in orange. OTS, octadecyltrichlorosilane; APTES, aminopropyltriethoxysilane. **e**, AFM image of an array of ferritin molecules. The bottom-right inset shows an AFM phase image of a section containing individual ferritin molecules. The space within the arrows is 10 nm. The top-right inset illustrates the structure of the ferritin. The polypeptide shell of the protein is shown in blue. Figure reprinted with permission from: **b**, ref. 42, © Royal Society of Chemistry; **c**, ref. 97, © American Chemical Society; **d**,**e**, ref. 6, © Wiley.

by the quantum dot. The differential conductance as a function of the source and gate voltages shows the characteristic Coulomb diamond structure (Fig. 6f).

Additional SPL methods

The versatility of force microscopy to modify and manipulate surfaces (Fig. 1b) has generated some other approaches such as nanomachining[104], nanoscale dispensing[105] or dip-pen nanolithography[106]. Mechanical SPL (nanomachining) uses the mechanical force exerted by the tip to induce the selective removal of material from a surface. It has been successfully applied to modify solid substrates[107] and films of polymers[108]. The same approach has also been used for the local removal of parts of self-assembled monolayers and Langmuir–Blodgett films (nanoshaving)[109]. The limiting factor in creating reproducible patterns is the stability of the tip, which is prone to deformation and contamination from the debris of the removed material.

Nanoscale dispensing uses hollow cantilevers comprising integrated fluidic channels to deliver small liquid drops onto a surface[110]. The fluidic channel allows soluble molecules to be dispensed through the hollow AFM tip. One remarkable application of nanoscale dispensing has been the stimulation of single living cells under physiological conditions[105].

Dip-pen SPL (dp-SPL) offers high resolution and registration with direct write patterning capabilities[106]. This lithography functions by facilitating the direct transport of molecules to surfaces, much like the transfer of ink from a macroscopic dip-pen to paper. By depositing several different kinds of molecule on the same substrate, dp-SPL can pattern a range of desired chemistries with sub-100-nm control. Dip-pen SPL is compatible with a variety of inks, including organic and biological[111] molecules, polymers, colloidal particles and metal ions. The intrinsic linear writing speed of dp-SPL depends on molecular transport between the probe tip and the surface, and thus it is limited by mass diffusion. The tip temperature can be used to control the ink deposition[112]. The rise of the temperature of the tip causes solid ink to melt and wet the tip. The advantage of this approach is twofold. The ink flow can be turned on and off at will whereas previous dp-SPL techniques apply ink to the surface as long as the tip stays in contact with it. Furthermore, the rate of the ink diffusion is tunable by controlling the tip temperature. It has been shown that poly(*N*-isopropylacrylamide), a type of protein adhesion molecule, can be reproducibly written from the melt[112]. These nanostructures reversibly bind and release proteins when actuated through the hydrophilic–hydrophobic phase transition. This approach has also been applied to fabricate graphene nanorribons[113].

© 2014 Macmillan Publishers Limited. All rights reserved

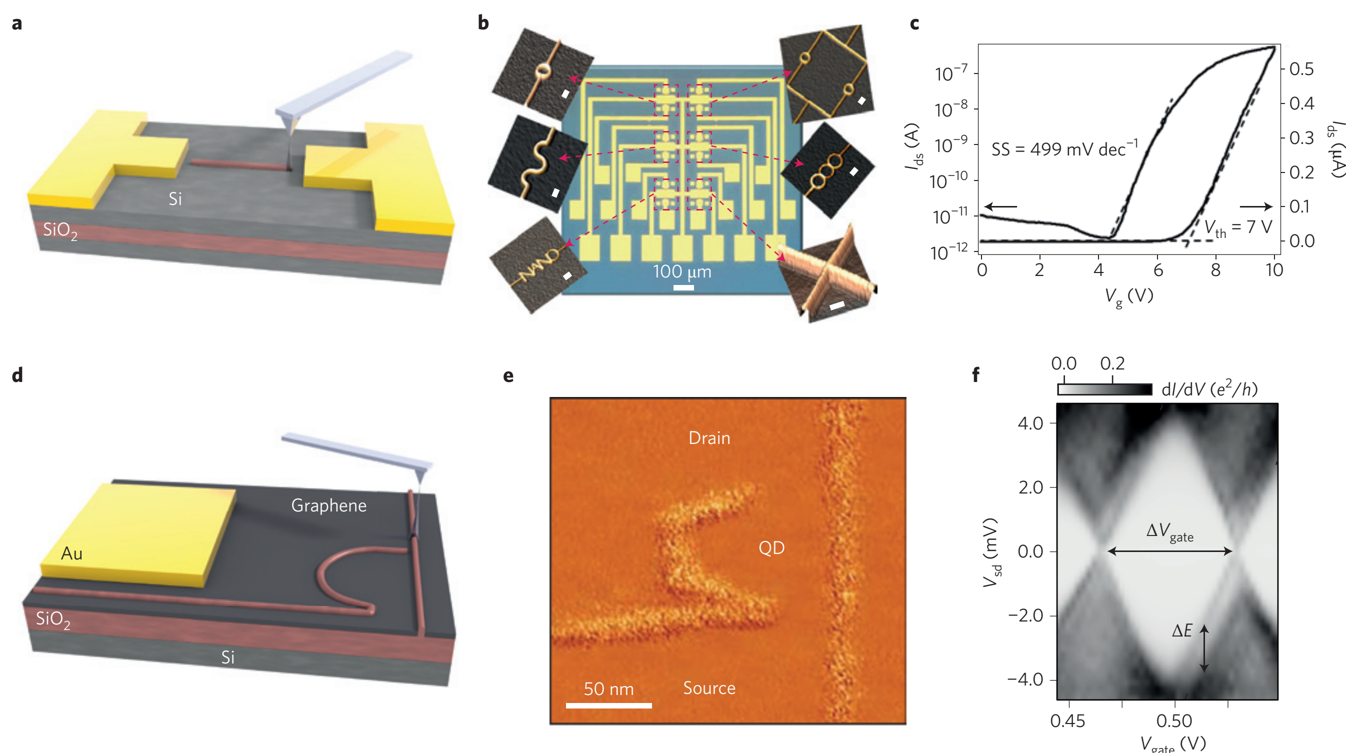

Figure 6 | Silicon and graphene nanolectronic devices fabricated by oxidation scanning probe lithography. a, Scheme of the fabrication of a very thin and narrow oxide mask. That mask defines the width of a silicon nanowire. **b**, Atomic force microscopy images of silicon nanowires of different geometries fabricated by oxidation SPL (o-SPL). The image of the gold pads and connections has been obtained by optical microscopy. Scale bars in the AFM images, 100 nm. **c**, Transfer characteristics of a silicon nanowire field-effect transitor made by o-SPL. SS, subthreshold swing; V_{th}, threshold voltage; V_g, gate voltage; I_{ds}, drain current. **d**, Scheme of the fabrication of a graphene quantum dot. A graphene layer deposited on a silicon dioxide film is locally oxidized by an atomic force microscope tip. **e**, Atomic force microscopy image of a single quantum dot (QD). **f**, Coulomb blockade diamond of the quantum dot measured at $T = 50$ mK. Figure reprinted with permission from: **b**, ref. 15, © Institute of Physics; **c**, ref. 102, © Institute of Physics; **e**,**f**, ref. 90, © American Institute of Physics.

Large-area patterning

One of the main drawbacks of SPL techniques for technological oriented applications is the limited throughput due to the serial writing process and the required interaction timescales (Fig. 2b). Recent developments in wide-area-operation high-speed AFM[30,114] could enhance the serial writing and imaging speed, if the pixel times are not limited by the physics of the writing process. More effectively, parallelization could enhance the throughput by a factor proportional to the number of cantilevers operating in parallel. Functional parallel probe arrays have been demonstrated in a variety of schemes ranging from fully passive systems with no actuation control and read-out capability at the individual cantilever level to fully controlled systems at the individual cantilever level. For fully passive systems, dp-SPL has demonstrated parallel operation of 55,000 levers replicating the same nanostructures[115]. A more recent intermediate step without integrated read-out employs active write control by either thermal expansion or optical addressability for polymer-pen lithography[116] and beam-pen optical lithography[117], respectively. These systems have shown the ability to pattern cm^2 areas, however, *in situ* inspection is difficult and resolution is limited.

A typical single-cantilever AFM employs an optical-lever deflection scheme that cannot be easily scaled up to large cantilever arrays due to the complexity in the optical set-up, signal processing and restrictions on cantilever geometries[118]. For fully controlled parallel systems integration of actuators and sensors into the individual cantilevers is required. For a recent review of actuation and sensing schemes see ref. 119. At least three terminals are needed per cantilever to control read and write processes separately, which poses an integration challenge for high numbers of parallel levers. Such a fully integrated parallel system was developed for thermomechanical data-storage applications by IBM demonstrating parallel read and write operation at 32-nm full-pitch resolution[120]. The tool used a similar cantilever design as shown in Fig. 3a solving the integration challenge by transfer of the cantilevers onto a complementary metal–oxide–semiconductor chip. Both t-SPL and tc-SPL could directly benefit from the array technology developed for the data-storage application. Array sizes up to 64 × 64 cantilevers have been achieved, which would lead to a throughput increase by a factor of more than 4,000. Together with the high linear speed of t-SPL, throughput values of >10^8 µm^2 h^{-1} are within reach, which would open up new application fields such as nanoimprint master or optical mask fabrication.

Recently, parallel operation of a five-tip array for tc-SPL was demonstrated in a commercial AFM set-up (Fig. 4e)[22]. The same array is used *in situ* to pattern and image microstructures, nanowires and complex patterns of a conjugate luminescent semiconducting polymer (Fig. 4e), as well as conductive nanoribbons of reduced graphene oxide. Resolution down to sub-50 nm over areas of 500 µm^2 and parallel complex three-dimensional patterning of conjugated polymers have been demonstrated.

Large-area patterning has also been addressed by using printing-based methods. Here, the use of a stamp facilitates the upscaling of the processes involved in some SPL methods[61,74,121,122]. In this approach, a single patterning step, say anodic oxidation in o-SPL, is replicated multiple times by using a stamp containing billions of nanostructures. The contact electrochemical replication scheme has enabled the patterning of alternating hydrophobic/hydrophilic

© 2014 Macmillan Publishers Limited. All rights reserved

domains on octadecyltrichlorosilane monolayers[122]. However, in this approach the positioning capabilities of SPL are lost.

Outlook

Scanning probe lithography has experienced a quiet evolution over the past twenty years. Scanning probe lithography techniques offer a variety of physical and chemical approaches to modify a surface, giving rise to a wealth of methods for patterning. These methods have drawn considerable scientific attention for different reasons. On one hand, SPL is an alternative method to pattern surfaces or devices with nanoscale precision. On the other hand, SPL enables access to phenomena at the nanoscale with an easiness that is not paralleled by other techniques. Those features, together with the wide range of materials that can be patterned, the ability to pattern in ambient conditions and the relatively few requirements to transform a conventional AFM into a nanolithography instrument explain the interest and relevance of SPL in the scientific community. An illuminating example of the versatility of SPL is the recent nanofabrication of devices based on novel two-dimensional materials.

The interest and use of SPL in scientific research is established and expanding, however more technological applications still need to be fulfilled. To progress out of the research environment and into a technology used for prototyping applications, the method has to achieve sufficient throughput and reliability for day-to-day work. Some milestones towards this goal have been achieved just recently. In particular, the closed-loop-lithography framework may lead to SPL tools that operate autonomously and thus with minimal learning and preparation overhead for the user. The particular strength of SPL systems of giving the user a direct feedback on the result of the operation will play a major role in the success of commercial systems. Other challenges are still to be resolved. Most prominently, parallelization and tip lifetime, which although greatly enhanced for the approaches discussed in this Review, still need to be extended to meet user needs for patterning cm^2 areas at high speeds, high resolution and high reproducibility.

The tip lifetime defined in terms of its chemical nature and geometry is a factor that controls and determines both the reproducibility and the throughput in SPL. This Review provides an update of SPL methods based on either physical or chemical processes that better preserve the tip's geometry and chemical nature. For physical processes, this is because the force is exerted over polymers with elastic moduli orders of magnitude smaller than those of the tip materials; for chemical processes, this is because the process happens mostly on the sample surface.

The limited throughput of SPL methods is being addressed by two different approaches. The first involves the use of arrays of several SPL cantilevers, which can write and read in parallel. In SPL, the actuation and topography sensing scheme can be implemented into the cantilever, which occupies an area of less than $100 \times 100\ \mu m^2$. This is a unique and ideal condition for parallelization. Furthermore, the resolution is typically determined by the shape of the tip and thus it is not impaired by the existence of neighbouring levers. Thus, in SPL parallelization the resolution is conserved while the throughput scales linearly with the number of cantilevers. The major challenges towards a highly parallel system are engineering tasks for the reliable fabrication of cantilever arrays and for a solution of the wiring problem. Both can be solved as it has been demonstrated in IBM's probe data-storage project or in other more recent demonstrations of linear arrays of thermal cantilevers. In the near future, it is expected that linear arrays of 30 thermal cantilevers can be integrated in a commercial AFM, with the goal of writing and then reading more than 1 million pixels in 1 second. Because the distance between the cantilevers in the array is 100 μm, and the scan range of commercial AFMs is typically about 100 μm, 30 cantilevers will be able to nanopattern 3 mm × 0.1 mm in a single patterning action. Larger areas could be addressed by moving the sample and using fast stitching procedures. For example, with existing technology SPL could produce graphene nanoribbons on functionalized graphene at speeds 10^4 times faster than electron-beam lithography. The second approach is less sophisticated, and it is based on replicating the processes involved in SPL by using micro or nanopatterned stamps.

The capability of the force microscope to provide chemical and nanomechanical information at the atomic[123], molecular and nanoscale[124,125] levels could also be incorporated in the SPL methodology. Those methods could provide an *in situ* determination of the physical and chemical properties of the fabricated nanostructures. This is another factor that will support the evolution and expansion of SPL.

In conclusion, SPL is approaching a stage where proof-of-principle academic experiments can become widespread technology. The large variety of materials that can be patterned by SPL, from polymers to proteins to graphene, the high resolution, the ability to work in a range of environmental conditions, from liquid to air and vacuum, and the potential to pattern chemistry and topography simultaneously make SPL an attractive nanofabrication method for the next generation of materials and devices.

Received 3 April 2014; accepted 4 July 2014;
published online 5 August 2014

References

1. Saavedra, H. M. *et al.* Hybrid strategies in nanolithography. *Rep. Prog. Phys.* **73,** 036501 (2010).
2. Acikoz, C., Hempenius, M. A., Huskens, J. & Vancso, G. J. Polymers in conventional and alternative lithography for the fabrication of nanostructures. *Eur. Poly. J.* **47,** 2033–2052 (2011).
3. Lipson, A. L. & Hersam, M. C. Conductive scanning probe characterization and nanopatterning of electronic and energy materials. *J. Phys. Chem. C* **117,** 7953–7963 (2013).
4. Pires, D. *et al.* Nanoscale three-dimensional patterning of molecular resists by scanning probes. *Science* **328,** 732–735 (2010).
First implementation of precise three-dimensional relief patterning using thermal scanning probe lithography.
5. Fuechsle, M. *et al.* A single-atom transistor. *Nature Nanotech.* **7,** 242–246 (2012).
6. Martinez, R. V. *et al.* Large-scale nanopatterning of single proteins used as carriers of magnetic nanoparticles. *Adv. Mater.* **22,** 588–591 (2010).
7. *International Technology Roadmap for Semiconductors 2013 Edition, Lithography Summary*; http://www.itrs.net/Links/2013ITRS/2013Chapters/2013Litho_Summary.pdf (2013).
8. Tennant, D. M. in *Nanotechnology* (ed. Timp, G.) Ch. 4, 161–205 (Springer, 1999).
9. Van Oven, J., Berwald, F., Berggren, K., Kruit, P. & Hagen, C. Electron-beam-induced deposition of 3-nm-half-pitch patterns on bulk Si. *J. Vac. Sci. Technol. B* **29,** 06F305 (2011).
10. de Boer, G. *et al.* MAPPER: progress toward a high-volume manufacturing system. *Proc. SPIE* **8680,** 86800O (2013).
11. Gubiotti, T. *et al.* Reflective electron beam lithography: lithography results using CMOS controlled digital pattern generator chip. *Proc. SPIE* **8680,** 86800H (2013).
12. van der Drift, E. & Maas, D. J. in *Nanotechnology* (eds Stepanova, M. & Dew, S.) Ch. 4, 93–116 (Springer, 2012).
13. Gonzalez, C. M. *et al.* Focused helium and neon ion beam induced etching for advanced extreme ultraviolet lithography mask repair. *J. Vac. Sci. Technol. B* **32,** 021602 (2014).
14. Lin, Y. C. *et al.* Graphene annealing: how clean can it be? *Nano Lett.* **12,** 414–419 (2012).
15. Martinez, R. V., Martinez, J. & Garcia, R. Silicon nanowire circuits fabricated by AFM oxidation nanolithography. *Nanotechnology* **21,** 245301 (2010).
16. Weng, L., Zhang, L., Chen, Y. P. & Rokhinson, L. P. Atomic force microscope local oxidation nanolithography of graphene. *Appl. Phys. Lett.* **93,** 093107 (2008).
17. Kim, S. *et al.* Direct fabrication of arbitrary-shaped ferroelectric nanostructures on plastic, glass, and silicon substrates. *Adv. Mater.* **23,** 3786–3790 (2011).
18. Wang, D. *et al.* Direct writing and characterization of poly(*p*-phenylene vinylene) nanostructures. *Appl. Phys. Lett.* **95,** 233108 (2009).
19. Fenwick, O. *et al.* Thermochemical nanopatterning of organic semiconductors. *Nature Nanotech.* **4,** 664–668 (2009).

© 2014 Macmillan Publishers Limited. All rights reserved

20. Carroll, K. M. *et al.* Fabricating nanoscale gradients with thermochemical nanolithography. *Langmuir* **29,** 8675–8682 (2013).
21. Felts, J. R., Onses, M. S., Rogers, J. A. & King, W. P. Nanometer scale alignment of block-copolymer domains by means of a scanning probe tip. *Adv. Mater.* **26,** 2999–3002 (2014).
22. Carroll, K. M. *et al.* Parallelization of thermochemical nanolithography. *Nanoscale* **6,** 1299–1304 (2014).
23. Mamin, H. & Rugar, D. Thermomechanical writing with an atomic force microscope tip. *Appl. Phys. Lett.* **61,** 1003–1005 (1992).
24. King, W. P. *et al.* Heated atomic force microscope cantilevers and their applications. *Annu. Rev. Heat Transfer* **16,** 287–326 (2013).
Review on scanning probe microscopy and lithography using heatable tips.
25. Szoszkiewicz, R. *et al.* High-speed, sub-15 nm feature size thermochemical nanolithography. *Nano Lett.* **7,** 1064–1069 (2007).
Example of the capabilities of thermochemical scanning probe lithography for high resolution and fast nanopatterning.
26. Gotsmann, B., Duerig, U., Frommer, J. & Hawker, C. J. Exploiting chemical switching in a Diels-Alder polymer for nanoscale probe lithography and data storage. *Adv. Funct. Mater.* **16,** 1499–1505 (2006).
27. Cheong, L. L. *et al.* Thermal probe mask-less lithography for 27.5 nm half-pitch Si technology. *Nano Lett.* **13,** 4485–4491 (2013).
28. Knoll, A. W. *et al.* Probe-based 3-D nanolithography using self-amplified depolymerization polymers. *Adv. Mater.* **22,** 3361–3365 (2010).
29. Paul, P., Knoll, A., Holzner, F., Despont, M. & Duerig, U. Rapid turnaround scanning probe nanolithography. *Nanotechnology* **22,** 275306 (2011).
30. Paul, P., Knoll, A., Holzner, F. & Duerig, U. Field stitching in thermal probe lithography by means of surface roughness correlation. *Nanotechnology* **23,** 385307 (2012).
31. Shaw, J. E., Stavrinou, P. N. & Anthopoulos, T. D. On-demand patterning of nanostructured pentacene transistors by scanning thermal lithography. *Adv. Mater.* **25,** 552–558 (2013).
On-demand patterning of field-effect transistors from a pentacene precursor by thermal scanning probe lithography.
32. Wei, Z. *et al.* Nanoscale tunable reduction of graphene oxide for graphene electronics. *Science* **328,** 1373–1376 (2010).
33. Lee, W.-K. *et al.* Nanoscale reduction of graphene fluoride via thermochemical nanolithography. *ACS Nano* **7,** 6219–6224 (2013).
34. Duvigneau, J., Schoenherr, H. & Vancso, G. J. Atomic force microscopy based thermal lithography of poly(tert-butyl acrylate) block copolymer films for bioconjugation. *Langmuir* **24,** 10825–10832 (2008).
35. Wang, D. *et al.* Thermochemical nanolithography of multifunctional nanotemplates for assembling nano-objects. *Adv. Funct. Mater.* **19,** 3696–3702 (2009).
36. Holzner, F. *et al.* Directed placement of gold nanorods using a removable template for guided assembly. *Nano Lett.* **11,** 3957–3962 (2011).
37. Holzner, F. *et al.* High density multi-level recording for archival data preservation. *Appl. Phys. Lett.* **99,** 023110 (2011).
38. Torrey, J. *et al.* Scanning probe direct-write of germanium nanostructures. *Adv. Mater.* **22,** 4639–4642 (2010).
39. Garcia, R. *et al.* Nanopatterning of carbonaceous structures by field-induced carbon dioxide splitting with a force microscope. *Appl. Phys. Lett.* **96,** 143110 (2010).
40. Suez, I. *et al.* High-field scanning probe lithography in hexadecane: Transitioning from field induced oxidation to solvent decomposition through surface modification. *Adv. Mater.* **19,** 3570–3573 (2007).
41. Dagata, J. A. *et al.* Modification of hydrogen-passivated silicon by a scanning tunneling microscope operating in air. *Appl. Phys. Lett.* **56,** 2001–2003 (1990).
42. Garcia, R., Martinez, R. V. & Martinez, J. Nanochemistry and scanning probe nanolithographies. *Chem. Soc. Rev.* **35,** 29–38 (2006).
43. Yan, N. *et al.* Water-mediated electrochemical nano-writing on thin ceria films. *Nanotechnology* **25,** 075701 (2014).
44. Li, Y., Maynor, B. W. & Liu, J. Electrochemical AFM 'dip-pen' nanolithography. *J. Am. Chem. Soc.* **123,** 2105–2106 (2001).
45. Arruda, T. M. *et al.* Toward quantitative electrochemical measurements on the nanoscale by scanning probe microscopy: Environmental and current spreading effects. *ACS Nano* **7,** 8175–8182 (2013).
46. Wei, Y. M. *et al.* The creation of nanostructures on an Au(111) electrode by tip-induced iron deposition from an ionic liquid. *Small* **4,** 1355–1358 (2008).
47. Obermair, C., Kress, M., Wagner, A. & Schimmel, T. Reversible mechano-electrochemical writing of metallic nanostructures with the tip of an atomic force microscope. *Beilstein J. Nanotech.* **3,** 824–830 (2012).
48. Zhang, K. *et al.* Direct writing of electronic devices on graphene oxide by catalytic scanning probe lithography. *Nature Commun.* **3,** 1194 (2012).
49. Liu, J.-F. & Miller, G. P. Field-assisted nanopatterning of metals, metal oxides and metal salts. *Nanotechnology* **20,** 055303 (2009).
50. Ferris, R. *et al.* Field-induced nanolithography for patterning of non-fouling polymer brush surfaces. *Small* **7,** 3032–3037 (2011).
51. Kaestner, M., Hofer, M. & Rangelow, I. W. Nanolithography by scanning probes on calixarene molecular glass resist using mix-and-match lithography. *J. Micro/Nanolith. MEMS MOEMS* **12,** 031111 (2013).
52. Lyuksyutov, S. F. *et al.* Electrostatic nanolithography in polymers using atomic force microscopy. *Nature Mater.* **2,** 468–472 (2003).
53. Lyding, J. W., Shen, T. C., Hubacek, J. S., Tucker, J. R. & Abeln, G. C. Nanoscale patterning and oxidation of H-passivated Si(100)-2×1 surfaces with an ultrahigh-vacuum scanning tunneling microscope. *Appl. Phys. Lett.* **64,** 2010–2012 (1994).
54. Blanco, E. M., Nesbitt, S. A., Horton, M. A. & Mesquida, P. A multiprotein microarray on silicon dioxide fabricated by using electric-droplet lithography. *Adv. Mater.* **19,** 2469–2473 (2007).
55. Cho, Y., Hashimoto, S., Odagawa, N., Tanaka, K. & Hiranaga, Y. Nanodomain manipulation for ultrahigh density ferroelectric data storage. *Nanotechnology* **17,** S137–S141 (2006).
56. Tayebi, N. *et al.* Tuning the built-in electric field in ferroelectric $Pb(Zr_{0.2}Ti_{0.8})O_3$ films for long-term stability of single-digit nanometer inverted domains. *Nano Lett.* **12,** 5455–5463 (2012).
57. Weber, B. *et al.* Ohm's law survives to the atomic scale. *Science* **335,** 64–67 (2012).
58. Weber, B., Mahapatra, S., Watson, T. & Simmons, M. Y. Engineering independent electrostatic control of atomic-scale (~4 nm) silicon double quantum dots. *Nano Lett.* **12,** 4001–4006 (2012).
59. Tayebi, N. *et al.* An ultraclean tip-wear reduction scheme for ultrahigh density scanning probe-based data storage. *ACS Nano* **4,** 5713–5720 (2010).
60. Forrester, M. *et al.* Charge-based scanning probe readback of nanometer-scale ferroelectric domain patterns at megahertz rates. *Nanotechnology* **20,** 225501 (2009).
61. Martinez, R. V., Losilla, N. S., Martinez, J. & Garcia, R. Patterning polymeric structures with 2 nm resolution at 3 nm half pitch in ambient conditions. *Nano Lett.* **7,** 1846–1850 (2007).
This contribution reports the smallest periodic pattern fabricated on silicon at atmospheric pressure and room temperature.
62. Vasko, S. E. *et al.* Serial and parallel Si, Ge, and SiGe direct-write with scanning probes and conducting stamps. *Nano Lett.* **11,** 2386–2389 (2011).
63. Lyo, I. W. & Avouris, P. Field-induced nanometer-scale to atomic-scale manipulation of silicon surfaces with the STM. *Science* **253,** 173–176 (1991).
64. Eigler, D. M. & Schweizer, E. K. Positioning single atoms with a scanning tunneling microscope. *Nature* **344,** 524–526 (1990).
65. Custance, O., Perez, R. & Morita, S. Atomic force microscopy as a tool for atom manipulation. *Nature Nanotech.* **4,** 803–810 (2009).
Review on the use of the force microscope for atomic-scale manipulation.
66. Minne, S. C. *et al.* Centimeter scale atomic force microscope imaging and lithography. *Appl. Phys. Lett.* **73,** 1742–1744 (1998).
67. Lorenzoni, M. & Torre, B. Scanning probe oxidation of SiC, fabrication and kinetics considerations. *Appl. Phys. Lett.* **103,** 163109 (2013).
68. Kim, H. *et al.* Effects of ion beam irradiated Si on atomic force microscopy local oxidation. *Chem. Phys. Lett.* **566,** 44–49 (2013).
69. Zeira, A. *et al.* A bipolar electrochemical approach to constructive lithography: metal/monolayer patterns via consecutive site-defined oxidation and reduction. *Langmuir* **27,** 8562–8575 (2011).
70. Fabre, B. & Herrier, C. Automated sub-100 nm local anodic oxidation-directed nanopatterning of organic monolayer-modified silicon surfaces. *RSC Adv.* **2,** 168–175 (2012).
71. Meroni, D., Ardizzone, S., Schubert, U. S. & Hoeppener, S. Probe-based electro-oxidative lithography of OTS SAMs deposited onto transparent ITO substrates. *Adv. Funct. Mater.* **22,** 4376–4382 (2012).
72. Martin-Olmos, C. *et al.* Conductivity of SU-8 thin films through atomic force microscopy nano-patterning. *Adv. Funct. Mater.* **22,** 1482–1488 (2012).
73. Martinez, R. V. *et al.* Nanoscale deposition of single-molecule magnets onto SiO_2 patterns. *Adv. Mater.* **19,** 291–295 (2007).
74. Berson, J., Zeira, A., Maoz, R. & Sagiv, J. Parallel- and serial-contact electrochemical metallization of monolayer nanopatterns: A versatile synthetic tool *en route* to bottom-up assembly of electric nanocircuits. *Beilstein J. Nanotech.* **3,** 134–143 (2012).
Comprehensive study of the use of oxidation scanning probe lithography to pattern organic monolayers and their use as templates for the deposition of metallic nanoparticles.
75. Coronado, E. *et al.* Nanopatterning of anionic nanoparticles based on magnetic prussian-blue analogues. *Adv. Funct. Mater.* **22,** 3625–3633 (2012).
76. Khatri, O. P., Han, J., Ichiii, T., Murase, K. & Sugimura, H. J. Self-assembly guided one-dimensional arrangement of gold nanoparticles: A facile approach. *J. Phys. Chem. C* **112,** 16182–16185 (2008).
77. Oria, L., Ruiz de Luzuriaga, A., Alduncín, J. A. & Perez-Murano, F. Polystyrene as a brush layer for directed self-assembly of block co-polymers. *Microelec. Eng.* **110,** 234–240 (2013).

© 2014 Macmillan Publishers Limited. All rights reserved

78. Benetti, E. M., Chung, H. J. & Vancso, G. J. pH responsive polymeric brush nanostructures: Preparation and characterization by scanning probe oxidation and surface initiated polymerization. *Macromol. Rapid Commun.* **30,** 411–417 (2009).
79. Druzhinina, T. S., Hoeppener, C., Hoeppener, S. & Schubert, U. S. Hierarchical, guided self-assembly of preselected carbon nanotubes for the controlled fabrication of CNT structures by electrooxidative nanolithography. *Langmuir* **29,** 7515–7520 (2013).
80. Martin-Sanchez, J., Alonso-Gonzalez, P., Herranz, J., Gonzalez, Y. & Gonzalez, L. Site-controlled lateral arrangements of InAs quantum dots grown on GaAs(001) patterned substrates by atomic force microscopy local oxidation nanolithography. *Nanotechnology* **20,** 125302 (2009).
81. Delacour, C., Pannetier, B., Villegier, J. C. & Bouchiat, V. Quantum and thermal phase slips in superconducting niobium nitride (NbN) ultrathin crystalline nanowire: Application to single photon detection. *Nano Lett.* **12,** 3501–3506 (2012).
82. Yokoo, A., Tanabe, T., Kuramochi, E. & Notomi, M. Ultrahigh-*Q* nanocavities written with a nanoprobe. *Nano Lett.* **11,** 3634–3642 (2011).
83. Komijani, Y. *et al.* Origins of conductance anomalies in a p-type GaAs quantum point contact. *Phys. Rev. B* **87,** 245406 (2013).
84. Fuhrer, A. S. *et al.* Energy spectra of quantum rings. *Nature* **413,** 822–825 (2001).
85. Ubbelohde, N., Fricke, C., Hohls, F. & Haug, R. J. Spin-dependent shot noise enhancement in a quantum dot. *Phys. Rev. B* **88,** 041304 (2013).
86. Tsai, J. T. H., Hsu, C. H., Hsu, C. Y. & Yang, C. S. Rapid synthesis of gallium oxide resistive random access memory by atomic force microscopy local anodic oxidation. *Electron. Lett.* **49,** 554–555 (2013).
87. Schmidt, H., Rode, J. C., Belke, C., Smirnov, D. & Haug, R. J. Mixing of edge states at a bipolar graphene junction. *Phys. Rev. B* **88,** 075418 (2013).
88. Kurra, N., Reifenberger, R. G. & Kulkarni, G. U. Nanocarbon-scanning probe microscopy synergy: Fundamental aspects to nanoscale devices. *ACS Appl. Mater. Interf.* **6,** 6147–6163 (2014).
89. Byun, I. S. *et al.* Nanoscale lithography on monolayer graphene using hydrogenation and oxidation. *ACS Nano* **5,** 6417–6424 (2011).
90. Puddy, R. K., Chua, C. J. & Buitelaar, M. R. Transport spectroscopy of a graphene quantum dot fabricated by atomic force microscope nanolithography. *Appl. Phys. Lett.* **103,** 183117 (2013).
91. Neubek, S. *et al.* From one electron to one hole: Quasiparticle counting in graphene quantum dots determined by electrochemical and plasma etching. *Small* **6,** 1469–1473 (2010).
92. Masubuchi, S., Arai, M. & Machida, T. Atomic force microscopy based tunable local anodic oxidation of graphene. *Nano Lett.* **11,** 4542–4546 (2011).
93. Matsumoto, K., Gotoh, Y., Maeda, T., Dagata, J. A. & Harris, J. S. Room-temperature single-electron memory made by pulse-mode atomic force microscopy nano oxidation process on atomically flat α-alumina substrate. *Appl. Phys. Lett.* **76,** 239–241 (2000).
94. Snow, E. S. & Campbell, P. M. AFM fabrication of sub-10 nanometer metal-oxide devices with *in situ* control of electrical properties. *Science* **270,** 1639–1641 (1995).
One of the earliest applications of oxidation scanning probe lithography to fabricate nanoscale transistors.
95. Larki, F. *et al.* Pinch-off mechanism in double-lateral-gate junctionless transistors fabricated by scanning probe microscope based lithography. *Beilstein J. Nanotech.* **3,** 817–823 (2012).
96. Cavallini, M. *et al.* Additive nanoscale embedding of functional nanoparticles on silicon surface. *Nanoscale* **2,** 2069–2072 (2010).
97. Cramer, T., Zerbetto, F. & Garcia, R. Molecular mechanism of water bridge buildup: Field-induced formation of nanoscale menisci. *Langmuir* **24,** 6116–6120 (2008).
98. Skinner, L. B. *et al.* Structure of the floating water bridge and water in an electric field. *Proc. Natl Acad. Sci. USA* **109,** 16463–16468 (2012).
99. Calleja, M., Tello, M. & Garcia, R. Size determination of field-induced water menisci in noncontact atomic force microscopy. *J. Appl. Phys.* **92,** 5539–5542 (2002).
100. Kinser, C. R., Schmitz, M. J. & Hersam, M. C. Kinetics and mechanism of atomic force microscope local oxidation on hydrogen-passivated silicon in inert organic solvents. *Adv. Mater.* **18,** 1377–1380 (2006).
101. Maoz, R., Cohen, S. R. & Sagiv, J. Nanoelectrochemical patterning of monolayer surfaces: Toward spatially defined self-assembly of nanostructures. *Adv. Mater.* **11,** 55–61 (1999).
102. Ryu, Y. K., Chiesa, M. & Garcia, R. Electrical characteristics of silicon nanowire transistors fabricated by scanning probe and electron beam lithographies. *Nanotechnology* **24,** 315205 (2013).
103. Chiesa, M. *et al.* Detection of the early stage of recombinational DNA repair by silicon nanowire transistors. *Nano Lett.* **12,** 1275–1281 (2012).
104. Tseng, A. A. Removing material using atomic force microscopy with single- and multiple-tip sources. *Small* **7,** 3409–3427 (2011).
105. Meister, A. *et al.* FluidFM: Combining atomic force microscopy and nanofluidics in a universal liquid delivery system for single cell applications and beyond. *Nano Lett.* **9,** 2501–2507 (2009).
106. Salaita, K., Wang, Y. & Mirkin, C. A. Applications of dip-pen nanolithography. *Nature Nanotech.* **2,** 145–155 (2007).
107. Chen, H.-A., Lin, H.-Y. & Lin, H.-N. Localized surface plasmon resonance in lithographically fabricated single gold nanowires. *J. Phys. Chem. C* **114,** 10359–10364 (2010).
108. Shim, W. *et al.* Plow and ridge nanofabrication. *Small* **9,** 3058–3062 (2013).
109. Ngunjiri, J. & Garno, J. C. AFM-based lithography for nanoscale protein assays. *Anal. Chem.* **80,** 1361–1369 (2008).
110. Taha, H. *et al.* Protein printing with an atomic force sensing nanofountainpen. *Appl. Phys. Lett.* **83,** 1041–1043 (2003).
111. Bellido, E., de Miguel, R., Ruiz-Molina, D., Lostao, A. & Maspoch, D. Controlling the number of proteins with dip-pen nanolithography. *Adv. Mater.* **22,** 352–355 (2010).
112. Lee, W.-K., Whitman, L. J., Lee, J., King, W. P. & Sheehan, P. E. The nanopatterning of a stimulus-responsive polymer by thermal dip-pen nanolithography. *Soft Matter* **4,** 1844–1847 (2008).
113. Lee, W.-K. *et al.* Chemically isolated graphene nanoribbons reversibly formed in fluorographene using polymer nanowire masks. *Nano Lett.* **11,** 5461–5464 (2011).
114. Ando, T., Uchihashi, T. & Kodera, N. High-speed AFM and applications to biomolecular systems. *Annu. Rev. Biophys.* **42,** 393–414 (2013).
115. Mirkin, C. A. The power of the pen: Development of massively parallel dip-pen nanolithography. *ACS Nano* **1,** 79–83 (2007).
116. Eichelsdoerfer, D. J. Large-area molecular patterning with polymer pen lithography. *Nature Protoc.* **8,** 2548–2560 (2013).
117. Liao, X. *et al.* Desktop nanofabrication with massively multiplexed beam pen lithography. *Nature Commun.* **4,** 2103 (2013).
118. Koelmans, W. *et al.* Parallel optical readout of cantilever arrays in dynamic mode. *Nanotechnology* **21,** 395503 (2010).
119. Michels, T. & Rangelow, I. W. Review on scanning probe micromachining and its applications within nanoscience. *Microelectron. Eng.* http://dx.doi.org/10.1016/j.mee.2014.02.011 (2014).
120. Pantazi, A. *et al.* Probe-based ultrahigh-density storage technology. *IBM J. Res. Dev.* **52,** 493–511 (2010).
121. Cavallini, M. *et al.* Regenerable resistive switching in silicon oxide based nanojunctions. *Adv. Mater.* **24,** 1197–1201 (2012).
122. Zeira, A., Chowdhury, D., Maoz, R. & Sagiv, J. Contact electrochemical replication of hydrophilic-hydrophobic monolayer patters. *ACS Nano* **2,** 2554–2568 (2008).
123. Sugimoto, Y. *et al.* Chemical identification of individual surface atoms by atomic force microscopy. *Nature* **446,** 64–67 (2007).
124. Herruzo, E. T., Perrino, A. P. & Garcia, R. Fast nanomechanical spectroscopy of soft matter. *Nature Commun.* **5,** 3126 (2014).
125. Rice, R. H., Mokarian-Tabari, P., King, W. P. & Szoszkiewicz, R. Local thermomechanical analysis of a microphase-separated thin lamellar PS-b-PEO film. *Langmuir* **28,** 13503–13511(2012).
126. Holzner, F. *et al.* Thermal probe nanolithography: In-situ inspection, high-speed, high-resolution, 3D. *Proc. SPIE* **8886,** 888605 (2013).

Acknowledgements

Financial support from the European Research Council AdG no. 340177 (R.G.) and StG no. 307079 (A.W.K.), the European Commission FP7-ICT-2011 no. 318804 (R.G. and A.W.K.), the Swiss National Science Foundation SNSF no. 200020-144464 (A.W.K.), the Ministerio de Economía y Competitividad MAT2013-44858-R (R.G.), the National Science Foundation CMMI-1100290 (E.R.), the MRSEC program DMR-0820382 (E.R.) and the Office of Basic Energy Sciences of the Department of Energy DE-SC0002245 (E.R.) are acknowledged.

Additional information

Reprints and permissions information is available online at www.nature.com/reprints. Correspondence should be addressed to E.R.

Competing financial interests

The authors declare no competing financial interests.

© 2014 Macmillan Publishers Limited. All rights reserved